

LASERS

https://doi.org/10.1070/QEL16366

10-W mid-IR optical parametric oscillators based on $ZnGeP_2$ elements pumped by a fibre-laser-pumped Ho:YAG Laser. Experimental and numerical study

O.L. Antipov, I.D. Eranov, R.I. Kositsyn

Abstract. **The possibility of increasing the power and efficiency of 3.5–5.0 μm optical parametric oscillators (OPOs) based on one or two $ZnGeP_2$ crystals pumped by a repetitively pulsed Ho:YAG laser (λ = 2097 nm), which, in turn, is pumped by a thulium fibre laser (λ = 1908 nm), is studied. The OPO based on a tandem of $ZnGeP_2$ elements is demonstrated to generate high-quality beams with an average power up to 10 W in pulses with durations of 15–25 ns at a repetition rate of ~17 kHz. The total conversion efficiency of the fibre laser power to the mid-IR radiation reached 25%. A theoretical OPO model explaining a cluster spectrum and higher output power in the case of the $ZnGeP_2$ tandem than in the case of a single element is developed.**

Keywords: *mid-IR range, optical parametric oscillator, solid-state and fibre lasers, nonlinear optical crystal.*

1. Introduction

Mid-IR lasers operating at wavelength of 3–8 μm find numerous applications in medicine (for surgery and diagnostics), treatment of materials, ecological monitoring, remote analysis of material composition, control of industrial processes (in particular, in oil and gas processing), inspection of product pipelines, and other fields [1–3]. In the last decade, significant progress has been achieved in the development of high-power mid-IR optical parametric oscillators (OPOs) pumped by solid-state near-IR lasers [4–6]. One of the most attractive nonlinear crystals for parametric conversion is $ZnGeP_2$ (ZGP), whose advantages are high nonlinearity and thermal conductivity, as well as good transmission in a wide wavelength range (2.1–9 μm) [7–11]. To pump ZGP crystals, one can use Ho:YAG lasers pumped by fibre or solid-state lasers [12–15].

The aim of the present work was to evaluate the possibility of increasing the power and efficiency of mid-IR OPOs based on one or two ZGP nonlinear crystals and a pump Ho:YAG laser pumped by a thulium fibre laser with a wavelength of 1908 nm.

2. Experimental system

The mid-IR laser system consisted of two main parts: a pump laser based on Ho:YAG crystal and a ZGP OPO (Fig. 1).

O.L. Antipov, I.D. Eranov, R.I. Kositsyn Institute of Applied Physics, Russian Academy of Sciences, ul. Ul'yanova 46, 603950 Nizhnii Novgorod, Russia; e-mail: oleg_antipov@yahoo.com, 72ilya305@mail.ru, roman.kositsin@gmail.com

Received 17 March 2017; revision received 1 May 2017
Kvantovaya Elektronika **47** (7) 601–606 (2017)
Translated by M.N. Basieva

The Ho:YAG laser pumped by a Tm fibre laser was described in detail in [16]. The OPO was pumped by a repetitively-pulsed Ho:YAG laser with a wavelength of 2097 nm, a pulse repetition rate within the range of 5–40 kHz, a pulse duration of 20–30 nm, and a linear polarisation (with a power ratio between the vertically and horizontally polarised components higher than 100:1). The maximum power of the 2-μm Ho:YAG laser in experiments was restricted to 27 W to avoid breakdown of the nonlinear optical element (the pulse energy of the Ho:YAG laser did not exceed 3 mJ).

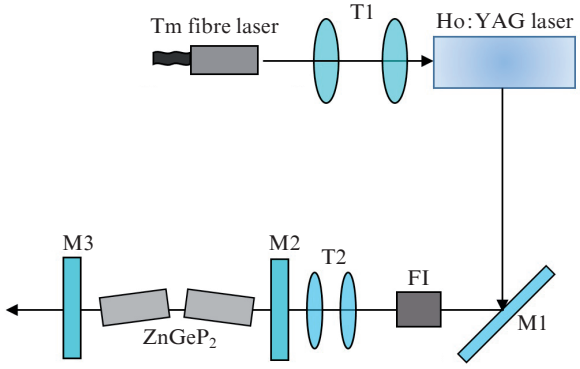

Figure 1. Scheme of the system: (T1) telescope for the Tm fibre laser radiation; (FI) Faraday isolator; (T2) telescope for the Ho:YAG laser radiation; (M1–M3) mirrors.

The Ho:YAG laser linewidth did not exceed 0.25 cm^{-1} (with an accuracy limited by the ~40-pm resolution of the OSA-23 spectrophotometer (Thorlabs, USA). This spectrophotometer did not allow us to resolve individual longitudinal modes, but, from the smoothness of laser pulses and extremely high OPO efficiency, we may conclude that the Ho:YAG laser operated in a single-mode regime. Indeed, the intermode interval $\Delta\nu = c/2L_{opt}$ (where c is the speed of light and L_{opt} is the total optical length of the cavity equal to ~140 mm) for the holmium laser was ~1 GHz. In the presence of several modes in the spectrum, the oscillogram of laser pulses in transient regimes exhibited beatings with a period of ~1 ns, which disappeared as the laser operation regime became stable with a pulse repetition rate of 17 kHz and an output power of 20–35 W.

Between the holmium laser cavity and the OPO, we placed a Faraday isolator FI. The holmium laser beam was focused into the OPO cavity centre using a two-lens telescope T2.

The OPO cavity was formed by two plane mirrors M2 and M3 spaced from each other by 20 mm or 42 mm in different

configurations. Mirror M2 had a high (above 98%) reflectance at wavelengths of 3–5 μm, while mirror M3 partially reflected two-micron radiation and had a transmittance of ~50% at wavelengths of 3.5–5 μm. The cavity contained one or two 8 × 5 × 5-mm active elements made of ZGP ('LOK' Ent., Tomsk, Russia). The crystals were cut at an angle $\varphi \approx 55°$ to the optical axis to achieve type-I phase matching (o–ee for positive crystals), and their faces were antireflection coated for the pump wavelength of 2.1 μm and the lasing wavelength of 3.5–5 μm. In the case of a tandem of ZGP crystals, the optical axes of the nonlinear elements were oppositely oriented to compensate for the walk-off of the ordinary pump wave from the extraordinary signal and idler waves of the OPO (Fig. 2). The OPO cavity length was 22 mm in the case of one nonlinear element and 43 mm for a tandem of ZGP elements.

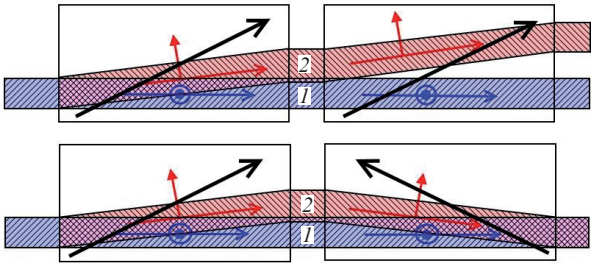

Figure 2. Trajectories of pump [shading from right to left, (*1*)] and generated [shading from left to right, (*2*)] beams and regions of their overlap (criss-cross shading) in cavities with walk-off compensation (bottom) and without it (top). The thick arrows indicate the orientations of optical axes; the thin arrows show the directions of beam propagation and polarization.

The beam waist diameter of 2-μm radiation in the OPO cavity was varied using a telescope from 900 to 1100 μm so that the pump energy density on the input face of the ZGP element did not exceed 0.4 J cm^{-2} to decrease the risk of its breakdown [17, 18].

3. Experimental results

The OPO pulses were recorded by home-made photodetectors based on PD 36-02-PR(TO18) and PD 48-03-NS-PR(TO18) photodiodes (OOO 'AIBI', St. Petersburg) with spectral response ranges of 1.5–3.8 and 3.8–4.8 μm, respectively. The FWHM duration of the OPO pulse (with a short leading edge) was 15–25 ns at a pump pulse duration of 25–30 ns (Fig. 3).

The conversion efficiency of the pump power to the OPO power depended on both the pump pulse repetition rate and the OPO power. The maximum output OPO power in the mid-IR range was obtained using a tandem of nonlinear elements at a pump power of 25 W and a pulse repetition rate of 17 kHz and reached 10 W (with a power efficiency of 41%) (Fig. 4). The output beams, whose structure was controlled using a PYROCAM III camera (Ophir-Spiricon, USA–Israel) with a filter transparent at λ = 3–5 μm, had homogeneous spatial distribution in the near- and far-field zones and a high quality close to the diffraction limit; the beam divergence at a wavelength of ~4.5 μm did not exceed 0.2 mrad at a beam diameter of 22 mm; the beam quality parameter was determined by the knife-edge method [19] to be $M^2 \leqslant 1.4$.

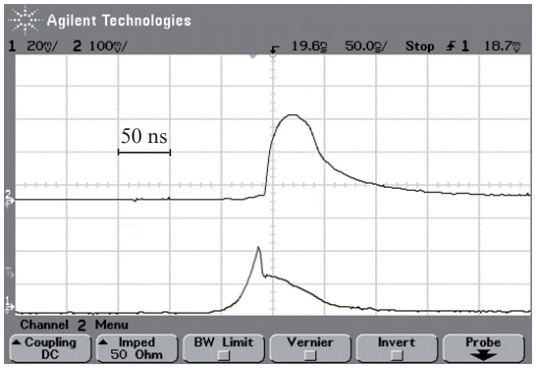

Figure 3. Oscillograms of (bottom) pump and (top) output OPO pulses near the threshold.

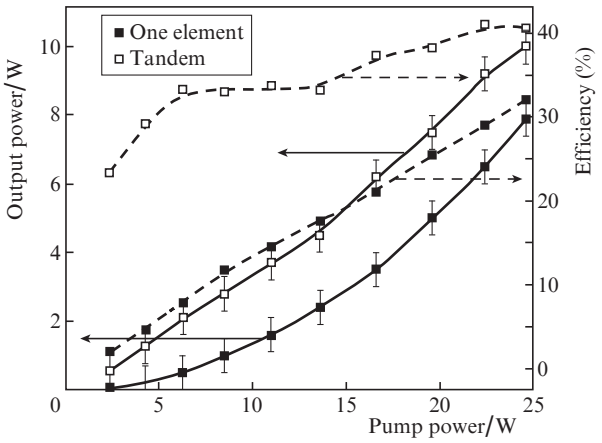

Figure 4. Dependences of the OPO output power (λ = 3–5 μm) (solid curves) and efficiency (dashed curves) on the pump power (λ = 2097 nm) in one-element and tandem configurations at a pulse repetition rate of 17 kHz.

The OPO spectrum recorded with an MDR-41 tunable monochromator (OKB 'Spektr', St. Petersburg) contained a series of lines peaking at λ = 3.8 and 4.5 μm, which corresponded to the signal and idler waves (Fig. 5). A similar cluster structure of a ZGP OPO spectrum was also previously

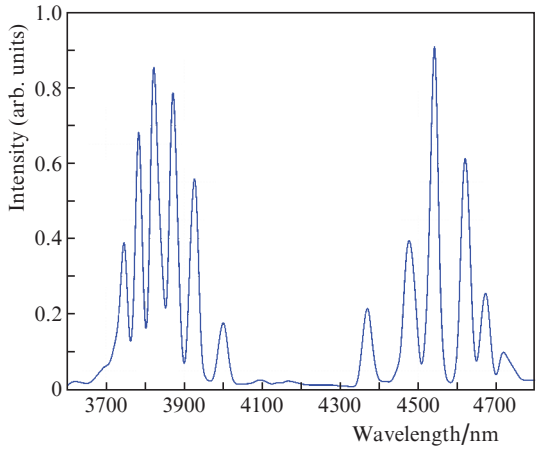

Figure 5. OPO spectrum measured using an MDR-41 monochromator with a step of 10 nm and an output slit width of 0.2 mm.

noted in [5, 6, 14]. According to classical works on the theory of two-cavity OPOs (see, for example, [20]), the laser lines at a significant excess over the threshold consist of clusters of modes, the single-pass phase difference for each of them being $\Delta\varphi = 2(k_p - k_s - k_i)L_N = 2\pi N$ (where k_q are the moduli of the wave vectors of the pump, signal, and idler waves, respectively; L_N is the length of the nonlinear element for the one-element configuration and the length of two elements for the tandem; and N is an integer). In the case of a single-frequency pump wave, to each signal wave mode there corresponds an idler wave mode for which the phase matching condition is satisfied in the best way.

4. Theoretical model of the OPO

The theoretical model of the OPO was developed on the assumption of single-mode single-frequency pumping, while the signal and idler waves were considered taking into account a set of longitudinal modes, each of them interacting only with the pump wave (a similar approach was previously developed for an OPO based on BBO crystals [21]). The experimental parameters and the characteristics of nonlinear ZGP elements used in the calculations are listed below.

Pump wavelength λ_p/nm	2097
Signal wavelength λ_s/nm	3800
Idler wavelength λ_i/nm	4680
Refractive index (at λ_p) n_p	3.14592 [22]
Refractive index (at λ_s) n_s	3.14833 [22]
Refractive index (at λ_i) n_i	3.14306 [22]
Phase matching angle θ/deg	.55
Walk-off angle ρ_w/mrad	.11.6
Absorption coefficient (at λ_p) α_p/cm^{-1}	.0.04
Absorption coefficient (at λ_s) α_s/cm^{-1}	.0.01
Absorption coefficient (at λ_i) α_i/cm^{-1}	.0.01
Reflectance of the OPO output mirror (at λ_p) R_p (%)	3
Reflectance of the OPO output mirror (at λ_s и λ_i) R (%)	.50
Nonlinear element length L_N/mm	.18
Pump beam waist radius r_p/μm	500
Temperature of the ZGP heat sink T_0/K	291
ZGP nonlinearity coefficient d_{36}/pm V^{-1}	69 [23], 70 [24], 75* [25]
Thermo-optic coefficient of ZGP (at λ_p) $(\partial n_p/\partial T)/10^{-6}$ K^{-1}	158.848 [22]
Thermo-optic coefficient of ZGP (at λ_s) $(\partial n_s/\partial T)/10^{-6}$ K^{-1}	162.47 [22]
Thermo-optic coefficient of ZGP (at λ_i) $(\partial n_i/\partial T)/10^{-6}$ K^{-1}	160.88 [22]
Thermal conductivity of ZGP K/W (cm K)$^{-1}$	0.36 [26]
Thermal conductivity of ZGP P/g cm^{-3}	4.12 [27]
ZPG heat capacity c_p/J g^{-1} K	.0.464 [27]
Longitudinal thermal expansion coefficient of ZPG $\beta_\parallel/10^{-6}$ K^{-1}	15.9 [28]
Transverse thermal expansion coefficient of ZPG $\beta_\perp/10^{-6}$ K^{-1}	17.5 [28]

* Calculations were performed for $d_{36} = 75$ pm V^{-1}.

Since the experiments revealed a good quality of the laser beams, we performed calculations in the approximation of Gaussian profiles of all beams (we also took into account the transverse walk-off of the extraordinary signal and idler waves with respect to the ordinary pump wave [29]):

$$E_q^{(j)\pm}(x,y,z,t) = c_q^{(j)\pm}(z,t) \times \exp\left(-\frac{r^2}{r_q^2(z)} - ik_q^{(j)}\frac{r^2}{2R_q(z)} + i\omega_q^{(j)}t \mp ik_q^{(j)}z - i\varphi_q^{(j)\pm}z\right) = c_q^{(j)\pm}(z,t)\exp[-i\varphi_q^{(j)\pm}(z) + i\omega_q^{(j)}t \mp i\Delta k^{(j)}z]\varepsilon_q(x,y,z), \quad (1)$$

where j is longitudinal mode number for the signal or idler wave; $E_q^{(j)\pm}$ is the electric field strength of waves propagating in the positive and negative direction of the z axis in the OPO; $c_q^{(j)\pm}$ is the electric field amplitude; $k_q^{(j)}$ is the mode wave vector; $\omega_q^{(j)}$ is the light wave frequency; $\Delta k^{(j)} = k_p - k_s^{(j)} - k_i^{(j)}$ is the mismatch for the jth mode; $\varphi_q^{(j)\pm}$ is the phase of the corresponding wave; $r_q(z)$ and $R_q(z)$ are the beam radius and the radius of curvature of the main transverse mode in the OPO cavity; $r^2 = (x - \rho_w z)^2 + y^2$; and ρ_w is the small walk-off angle for the extraordinary signal and idler waves (for the pump wave, $\rho_w = 0$). The signal and idler wavelengths and the walk-off angle were estimated from the phase matching conditions and the Sellmeier equation.

We numerically calculated the following system of truncated equations for wave powers $P_q^{(j)\pm}$ and eikonals ($\Phi^{(j)\pm} = \varphi_s^{(j)\pm} + \varphi_i^{(j)\pm} + \varphi_p^{(j)\pm}$) in the steady-state approximation (taking into account that the time of wave propagation over the OPO cavity length is small compared to the duration of light pulses) and on the assumption of a small walk-off of the signal and idler beams on the length of nonlinear interaction compared to the pump beam diameter:

$$\pm\frac{\partial P_s^{(j)\pm}}{\partial z} = -\gamma_s^{(j)}\sqrt{P_i^{(j)\pm}P_s^{(j)\pm}P_p^{\pm}} \times \sin(\Phi^{(j)\pm} + \Gamma \pm \Delta k^{(j)}z)J_\perp - \alpha_s P_s^{(j)\pm}, \quad (2)$$

$$\pm\frac{\partial P_i^{(j)\pm}}{\partial z} = -\gamma_i^{(j)}\sqrt{P_i^{(j)\pm}P_s^{(j)\pm}P_p^{\pm}} \times \sin(\Phi^{(j)\pm} + \Gamma \pm \Delta k^{(j)}z)J_\perp - \alpha_i P_i^{(j)\pm}, \quad (3)$$

$$\pm\frac{\partial P_p^{\pm}}{\partial z} = \sum_l \gamma_p^{(i)}\sqrt{P_i^{(l)\pm}P_s^{(l)\pm}P_p^{\pm}} \times \sin(\Phi^{(l)\pm} + \Gamma \pm \Delta k^{(l)}z)J_\perp - \alpha_p P_p^{\pm}, \quad (4)$$

$$\pm\frac{\partial \Phi_p^{(j)\pm}}{\partial z} + \left(\frac{2\pi i}{\lambda_p}\Delta n_p - \frac{2\pi i}{\lambda_s}\Delta n_s - \frac{2\pi i}{\lambda_i}\Delta n_i\right) = \sum_l\left[\gamma_p^{(l)}\cos(\Phi^{(l)\pm} + \Gamma \pm \Delta k^{(l)}z)\sqrt{\frac{P_i^{(l)\pm}P_s^{(l)\pm}}{P_p^{\pm}}}J_\perp\right] - \left(\gamma_s^{(j)}\sqrt{\frac{P_p^{\pm}P_i^{(j)\pm}}{P_s^{(j)\pm}}} + \gamma_i^{(j)}\sqrt{\frac{P_p^{\pm}P_s^{(j)\pm}}{P_i^{(j)\pm}}}\right) \times \cos(\Phi^{(j)\pm} + \Gamma \pm \Delta k^{(j)}z)J_\perp, \quad (5)$$

where

$$J_\perp \exp(i\Gamma) \equiv \frac{\int \varepsilon_p \varepsilon_s^* \varepsilon_i^* dxdy}{\sqrt{\int |\varepsilon_s|^2 dxdy \int |\varepsilon_i|^2 dxdy \int |\varepsilon_p|^2 dxdy}};$$

$$d_{eff} = 2d_{36}\sin(2\theta);$$

$$\gamma_{s,i,p}^{(j)} = \left(\frac{8\pi}{c}\right)^{3/2} \frac{1}{\sqrt{n_s n_i n_p}} \omega_{s,i,p}^{(j)} d_{eff} \left(\frac{\sin(\Delta\omega^{(j)}\tau_{res})}{\Delta\omega^{(j)}\tau_{res}}\right);$$

$$\Delta\omega^{(j)} = \omega_p - \omega_s^{(j)} - \omega_i^{(j)};$$

Δn_q is the change in the refractive index due to heating of the element; and $J_\perp$ and Γ are the amplitude and phase of the overlap integral. The coefficient $\sin(\Delta\omega^{(j)}\tau_{res})/(\Delta\omega^{(j)}\tau_{res})$ appears as a result of averaging the nonlinear term over the time of wave propagation through the OPO resonator τ_{res}.

Equations (2)–(5) took into account inverse conversion of the signal and idler wave energies (their nonlinear optical sum) into the backward travelling wave at $\lambda = 2100$ nm.

The boundary conditions for the powers of the pump and laser waves and eikonals had the form

$$P_p^+(z=0,t) = P_0(t),$$
$$P_p^-(z=L_N,t) = R_p P_p^+(z=L_N,t), \quad (6)$$

$$P_{s,i}^{+(j)}(z=0,t) = P_{s,i}^{-(j)}(z=0,t),$$
$$P_{s,i}^{-(j)}(z=L_N,t) = R P_{s,i}^{+(j)}(z=L_N,t), \quad (7)$$

$$\Phi^{(j)\mp}(z=(0,L_N),t) = \Phi^{(j)\pm}(z=(0,L_N),t) \quad (8)$$

$$+\left[\frac{P_{ns}}{P_s^{\pm(j)}(z=(0,L),t)} + \frac{P_{ni}}{P_i^{\pm(j)}(z=(0,L),t)}\right]\varphi_r + \frac{\Delta\omega^{(j)}}{c} L_{L,R},$$

$$\varphi_p^-(z=L_N,t) = \varphi_n,\ \varphi_p^-(z=0,t) = \varphi_{p,0}^-(t), \quad (9)$$

where R and R_p are the reflectances of the output mirror at the laser and pump wavelengths; $L_{L,R}$ are the lengths of the cavity regions from the input mirror to the nonlinear element and from the element to the output mirror; φ_r is the random quantum noise phase uniformly distributed from 0 to 2π;

$$P_{ns,ni} = \frac{hc^2}{2\lambda_{s,i} n_{s,i}(L_N + L_R + L_L)} \approx 4\times 10^{-10}\ \text{W} \quad (10)$$

are the average quantum noise powers per mode of the signal and idler waves on the nonlinear element faces [30, 31]; h is the Planck constant; and c is the speed of light in vacuum.

The initial condition for the complex amplitudes of the signal and idler modes was an arbitrary value with a uniform phase distribution (from 0 to 2π) and an average quantum noise power per mode determined by expression (10). We calculated the propagation of a pump pulse with a given duration and the Gaussian distribution at the input nonlinear element face $P_0(t) = P_0\exp[-(t - t_0)^2/\tau_p^2]$, where τ_p is the pump pulse duration. The scheme with two elements was calculated taking into account the walk-off of each wave between the elements. The spectrum of the longitudinal OPO modes was calculated for the cold cavity with account for the modes for which $\sin(\Delta\omega^{(j)}/\tau_{res})(\Delta\omega^{(j)}/\tau_{res})^{-1} > 0.1$ (the number of modes was varied, being, on average, 50).

In numerical calculations, we also took into account the influence of thermal effects in the crystal on the spatial distribution of the pump and laser beams, as well as the phases of waves. The thermal effects were analysed assuming that all the power absorbed in the crystal is spent on its heating. The temperature field was represented in the form of a sum of a time-averaged part (considered in the steady-state approximation) and additional heating during the pump pulse duration, which completely relaxed for the time between pulses. The equation for calculating the average part of the temperature field had the form

$$K\Delta T = \alpha_p\langle I_p(z)\rangle + \alpha_s\langle I_s(z)\rangle + \alpha_i\langle I_i(z)\rangle, \quad (11)$$

where $I_{s,i,p}$ is the intensity of corresponding waves and $\langle\ldots\rangle$ denotes averaging over several realisations. The boundary condition for Eqn (11) was a given temperature at the crystal boundary T_0. The equation for the change in temperature during the pulse was written as

$$\rho c_p \frac{\partial T}{\partial t} = \alpha_p I_p(z,t) + \alpha_s I_s(z,t) + \alpha_i I_i(z,t). \quad (12)$$

The found distribution was approximated by the parabola $\delta T(z,r) = \delta T_0(z) + T_2(z)r^2$. Heating of the element led to a change in its refractive index $\Delta n_q = (\partial n_q/\partial T)\delta T$, as well as to its thermal expansion (elongation) and to an increase in the difference in phase incursions $\beta_{eff}\delta T\Delta k^{(j)}L_N$, where $\beta_{eff} = \beta_\parallel \times \cos\theta + \beta_\perp\sin\theta$. The quadratic term in the refractive index variation along the transverse coordinate was accounted for as a thermal lens in the aberration-free approximation. In turn, this lens was taken into account when calculating the cavity mode by matrix optics methods, which determined the values of Γ and $J_\perp$ in Eqns (2)–(5).

The incidental factors taken into account in the calculations (noise seed phases, variations in the optical cavity length, number of modes) noticeably affected the calculation results, because of which we performed averaging over 100 realisations to obtain reliable data. Numerical calculations were performed for three OPOs: with one nonlinear element, with two consecutive elements without walk-off compensation, and with two elements with walk-off compensation (the optical axes were oriented as shown in Fig. 2). The dependences of the overlap integral $J_\perp$ on the longitudinal coordinate of the elements for these three cases are shown in Fig. 6.

5. Calculation results and comparison with the experiment

It is well known that the lasing wavelengths in a two-element OPO significantly depend on such system parameters as optical cavity length, nonlinear element temperature, etc. [20, 31]. Therefore, the optical cavity length in each of the numerical calculations was changed by an arbitrary value (the average of which was varied), which changed the mode composition and spectrum of the laser radiation. In this way, we took into account possible vibrations of the cavity mirrors and temperature fluctuations in the optical path. In the complete absence of random variations in the optical length, the OPO spectrum

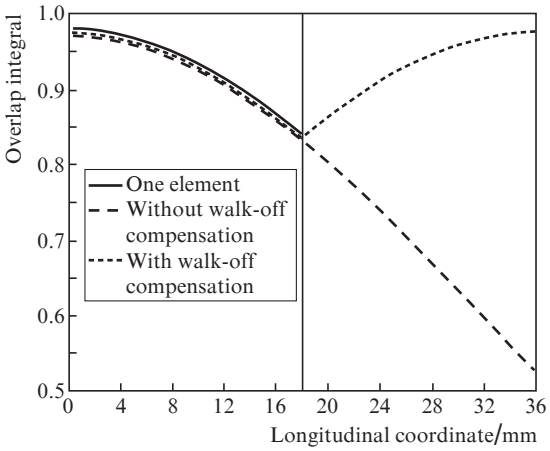

Figure 6. Dependences of the overlap integral on the coordinate along the element for three different OPO configurations. The vertical line in the centre indicates the boundary between the elements.

consisted of several lines, but they contained only a few modes and were too narrow compared to the experimentally measured lines. When the absolute change in the cavity length was equal to the pump wavelength, the spectrum consisted of two wide peaks without any components (Fig. 7). The best coincidence with the experiment was achieved at an arbitrary length deviation by ~100 nm. In this case, the OPO spectrum clearly shows separate mode clusters, which correspond to the quasi-phase-matching condition with a phase mismatch per pass divisible by 2π and have a width close to the experimental value. The absolute position of these cluster lines strongly depends on the cavity length and the pump wavelength, but their number and width at a given pump power remain constant. At the maximum pump power (24 W), the spectra of the signal and idler waves exhibit four clear lines; the number and widths of cluster lines decrease with decreasing pump power. Other calculations were also performed with averaging over many realisations with random changes in the cavity length, the average absolute value of these changes being 100 nm.

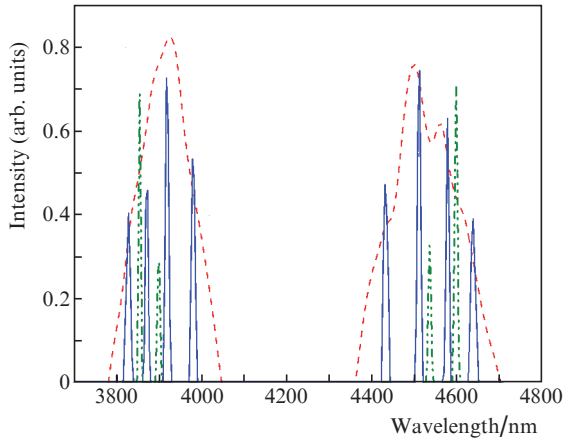

Figure 7. Calculated spectra of an OPO with random cavity length deviations of (dashed curve) 2000 and (solid curve) 100 nm at a pump power of 24 W, as well as (dot-and-dash curve) with cavity length deviations of 100 nm at a pump power of 10 W.

As a result of calculations, we obtained dependences of the OPO pulse power and mode composition on the pump power. The calculations of the output OPO power show that the efficiency of the OPO with two ZGP elements with walk-off compensation is higher than that in the OPO schemes without compensation and with one ZPG element (Fig. 8). At the same time, the lasing threshold in the one-element scheme was considerably higher. These results qualitatively agree with the experimental data (see Fig. 4), while the slightly (by no more than 15%) higher calculated output powers compared to experimental ones can be explained by ignored losses (for example, nonlinear losses inside the ZGP element [9, 11]), by a lower effective nonlinearity coefficient, or by the presence of several weak longitudinal modes of the pump wave.

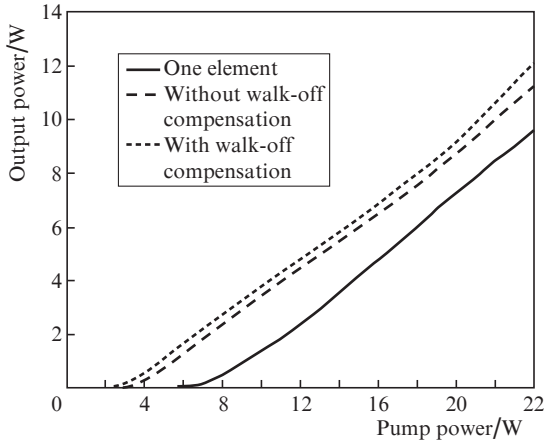

Figure 8. Numerically calculated dependences of the output OPO power on the pump power for three different OPO configurations.

We also numerically studied the dependences of the output OPO power, the passed pump power, and the power of the reconverted wave at the pump wavelength on the output mirror reflectance at a pump power of 24 W (Fig. 9). There exists an optimum (for the output power) reflectance in both one- and two-element OPO.

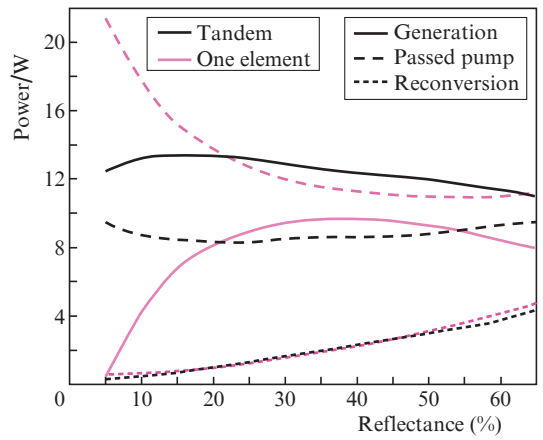

Figure 9. Numerically calculated dependences of the powers of (solid curves) OPO output, (dashed curves) passed pump radiation, and (dotted curves) reconverted wave at $\lambda = 2097$ nm on the output mirror reflectance for different OPO configurations.

This is explained by the fact that a decrease in the conversion efficiency at low reflectance is caused by insufficient gain per pass, while a decrease in the case of high reflectance occurs due to an increase in the efficiency of reconversion of the signal and idler waves. At the same time, the output power maximum of the tandem OPO is shifted to lower reflectances with respect to the maximum of the single-element OPO (due to a high gain per pass). The calculation results also show that one can obtain even a higher output power in an OPO cavity with a lower output mirror reflectance than that used in our experiments.

6. Conclusions

Thus, we have demonstrated the possibility of obtaining repetitively pulsed lasing in the wavelength range of 3.5–5 μm with an average power up to 10 W in an OPO based on a tandem of nonlinear optical elements made of $ZnGeP_2$ crystals. The efficiency of conversion of Ho:YAG laser radiation into radiation of the mid-IR OPO (with respect to the total average power of the idler and signal waves) reached 40%; the total conversion efficiency of the fibre laser power (λ = 1908 nm) into the mid-IR radiation was 25%. A theoretical OPO model is developed taking into account the output mode composition, the walk-off of beams in the nonlinear element and thermal effects. The numerical calculations of the OPO model have demonstrated good agreement with experimental results.

Acknowledgements. This work was partially supported by the Subprogramme of the Division of Physical Sciences of the Russian Academy of Sciences III.5 'New nonlinear optical materials, structures, and methods for designing laser systems with unique characteristics' (study of the OPO) and by the Russian Foundation for Basic Research (Project No. 15-42-0265, study of the Ho:YAG laser).

References

1. Sorokina I.T., Vodopyanov K.L. *Solid-State Mid-Infrared Sources* (Berlin–Heidelberg: Springer, 2003).
2. Ebrahim-Zadeh M., Sorokina I.T. *Mid-Infrared Coherent Sources and Applications* (Dordrecht: Springer, 2005).
3. Rudy C.W. *Laser Focus World*, **50** (5), 63 (2014).
4. Lippert E., Fonnum H., Arisholm G., Stenersen K. *Opt. Express*, **18** (25), 26475 (2010).
5. Hemming A., Richards J., Davidson A., et al. *Opt. Express*, **21** (8), 10062 (2013).
6. Yao B.Q., Shen Y.J., Duan X.M., et al. *Opt. Lett*., **39** (23), 6589 (2014).
7. Boyd G.D., Buehler E., Storz F.G. *Appl. Phys. Lett*., **18**, 301 (1971).
8. Andreev Yu.M., Voevodin V.G., Gibenyukov A.I., et al. *Sov. J. Quantum Electron*., **14**, 1021 (1984) [*Kvantovaya Elektron*., **11**, 1511 (1984)].
9. Schunemann P.G., Schepler K.L., Budni P.A. *MRS Bulletin*, **23**, 45 (1998).
10. Das S., Bhar G.C., Gangopadhyay S., Ghosh C. *Appl. Opt*., **42** (21), 4335 (2003).
11. Verozubova G.A., Gribenyukov A.I. *Crystallogr. Rep*., **53**, 158 (2008).
12. Budni P.A., Lemons M.L., Mosto J.R., Chicklis E.P. *IEEE J. Sel. Top. Quantum Electron*., **6**, 629 (2000).
13. Antipov O.L., Eremeykin O.N., Frolov Yu.N., et al. *Proc. Int. Symposium 'Topical Problems of Nonlinear Wave Physics' (NWP-2005)* (Nizhny Novgorod, 2005) p. 9.
14. Lippert E., Nicolas S., Arisholm G., et al. *Appl. Opt*., **45** (16), 3839 (2006).
15. Elder I. *Proc. SPIE*, **7325**, 73250I (2009).
16. Antipov O.L., Eranov I.D., Kositsyn R.I. *Laser Phys. Lett*., **14**, 015002 (2017).
17. Zawilski K.T., Setzler S.D., Schunemann P.G., Pollak T.M. *J. Opt. Soc. Am. B*, **23**, 2310 (2006).
18. Hildenbrand A., Kieleck C., Tyazhev A., et al. *Proc. SPIE*, **8964**, 896417 (2014).
19. GOST R ISO 11146-1-2008 'Lasers and laser-related equipment. Test methods for laser beam widths, divergence angles and beam propagation ratios. Part 1. Stigmatic and simple astigmatic beams.'
20. Eckardt R.C., Nabors C.D., Kozlovsky W.J., Byer R.L *J. Opt. Soc. Am. B*, **8** (3), 646 (1991).
21. Fix A., Wallenstein R. *J. Opt. Soc. Am. B*, **13** (11), 2484 (1996).
22. Kato K., Takaoka E., Umemura N. *Techn. Digest Conf. Lasers and Electrooptics CLEO/QELS 2003* (Washington, DC: OSA, 2003) paper CTuM17.
23. Roberts D.A. *IEEE J. Quantum Electron*., **28** (10), 2057 (1992).
24. Kato K. *Appl. Opt*., **36** (12), 2506 (1997).
25. Mason P.D., Jackson D.J., Gorton E.K. *Opt. Commun*., **110** (1), 163 (1994).
26. Beasley J.D. *Appl. Opt*., **33** (6), 1000 (1994).
27. Tucker J.E., Marquardt C.L., Bowman S.R., Feldman B.J. *Appl. Opt*., **34** (15), 2678 (1995).
28. Nikogosyan D.N. *Nonlinear Optical Crystals: a Complete Survey* (New York: Springer Science & Business Media, 2005).
29. Fleck J.A., Feit M.D. *J. Opt. Soc. Am*., **73** (7), 920 (1983).
30. Smith A.V., Alford W.J., Raymond T.D., Bowers M.S. *J. Opt. Soc. Am. B*, **12** (11), 2253 (1995).
31. Shen Y.R. *The Principles of Nonlinear Optics* (New York: John Wiley & Sons, 1984).